Chemistry Europe
European Chemical Societies Publishing

WILEY VCH

Excellence in Chemistry Research

Announcing our new flagship journal

- Gold Open Access
- Publishing charges waived
- Preprints welcome
- Edited by active scientists

Meet the Editors of *ChemistryEurope*

Luisa De Cola
Università degli Studi di Milano Statale, Italy

Ive Hermans
University of Wisconsin-Madison, USA

Ken Tanaka
Tokyo Institute of Technology, Japan

Check for updates

Chemistry–A European Journal
Research Article
doi.org/10.1002/chem.202300146
Chemistry Europe
European Chemical Societies Publishing
www.chemeurj.org

To Isomerize or not to Isomerize? *E*/*Z* Isomers of Cyclic Azobenzene Derivatives and Their Reactivity Upon One-Electron Reduction

Gabriel Glotz,[a] Konstantin Knaipp,[a] Martin S. Maier,[b] Katharina Hüll,[b] Alexander Novak,[b] Anne-Marie Kelterer,[a] Thomas Griebenow,[c] Rainer Herges,[c] Dirk Trauner,[d] and Georg Gescheidt*[a]

Abstract: Azo compounds are efficient electron acceptors. Upon one-electron reduction they generally isomerize forming the thermodynamically most stable radical anion. Herein we show that the size of the central ring in 1,2-diazocines and diazonines has a ruling influence on the configuration of the one-electron reduced species. Markedly, diazonines, which bear a central nine membered heterocycle, show light-induced *E*/*Z* isomerization, but retain the configuration of the diazene N=N moiety upon one-electron reduction. Accordingly, *E*/*Z* isomerization is not induced by reduction.

Introduction

Azo compounds have gained substantial relevance in technical and medical contexts. They can be selectively and reversibly switched between their *E*/*Z* isomers thermally or by irradiation at characteristic wavelengths. Whereas the *E* isomer reveals a 'stretched' arrangement of the two substituents at the central N=N moiety, the *Z* orientation causes a strain between two phenyl rings resulting in rather space-consuming (bulky) arrangement of the substituents. Accordingly, molecules comprising an azo moiety display unique properties depending on the prevailing isomer. This is for example, illustrated using azo moieties in self-healing polymers,[1–4] where switching between *E* and *Z* leads to an intrinsically differing topology causing remarkable macroscopic effects (softness/hardness of the material). The higher bulkiness of substituted *Z* isomers vs. the *E* is the basic principle in photopharmacology.[2,5–8] When azo moieties substituted with residues containing potential ligands are connected to transition-metal complexes in a way that the ligand atoms can interact with the metal cation depending on the prevailing *E* or *Z* isomer low- and high-spin states can selectively be populated. This finds applications particularly as switchable contrast agents[9–12] and in selective paramagnetic relaxation enhancement in NMR.[13]

Photoswitching requires a high quantum efficiency for the *E*↔*Z* isomerization and for obtaining a reasonable penetration depth (e.g., in blood-supported tissue), the wavelength required for the switching should be in the visible region, ideally within the so called "phototherapeutic window" (650–900 nm), and the absorption maxima of the two isomers should be well separated.

Accordingly, many derivatives based on the parent azobenzene (**1**) have been introduced. Bridged compounds (e.g. **2**–**8**, Scheme 1), are more stable in their *Z* arrangement.[14–20] This is a particular advantage because the "bulkier" *Z* isomers are generally inactive whereas the *E* isomers are sterically less demanding thus being the active forms in terms of binding to substrates. Accordingly, photo-induced *Z*↔*E* photoisomerization causes activation of functionalities in systems containing bridged azo moieties as photoresponsive units. Moreover, it has been shown that azo compounds with a strained geometry and those with aliphatic substituents form rather persistent radical ions upon one-electron reduction (or oxidation).[14,21–32] Whereas it has been shown that electron transfer causes efficient and rapid *Z*↔*E* conversion in non-bridged azo compounds with advantageous reduction potentials,[26,33–40] the changes in molecular configuration upon one-electron reduction in bridged azobenzene derivatives have not been addressed.

To obtain insights whether electron transfer is a likely pathway to induce *Z*↔*E* isomerization in bridged azo deriva-

[a] G. Glotz, K. Knaipp, Prof. A.-M. Kelterer, Prof. G. Gescheidt
Institute of Physical and Theoretical Chemistry
Graz University of Technology
Stremayrgasse 9/II, 8010 Graz (Austria)
E-mail: g.gescheidt-demner@tugraz.at
[b] Dr. M. S. Maier, Dr. K. Hüll, Dr. A. Novak
Department of Chemistry
New York University 100 Washington Square East
New York, NY 10003 (USA)
[c] T. Griebenow, Prof. R. Herges
Otto-Diels-Institute of Organic Chemistry
Christian Albrechts University Kiel
Otto Hahn Platz 4, 24118 Kiel (Germany)
[d] Prof. D. Trauner
Department of Chemistry
University of Pennsylvania
231 South 34th Street, Philadelphia, PA, 19104 (USA)

Supporting information for this article is available on the WWW under https://doi.org/10.1002/chem.202300146

© 2023 The Authors. Chemistry - A European Journal published by Wiley-VCH GmbH. This is an open access article under the terms of the Creative Commons Attribution Non-Commercial NoDerivs License, which permits use and distribution in any medium, provided the original work is properly cited, the use is non-commercial and no modifications or adaptations are made.

© 2023 The Authors. Chemistry - A European Journal published by Wiley-VCH GmbH

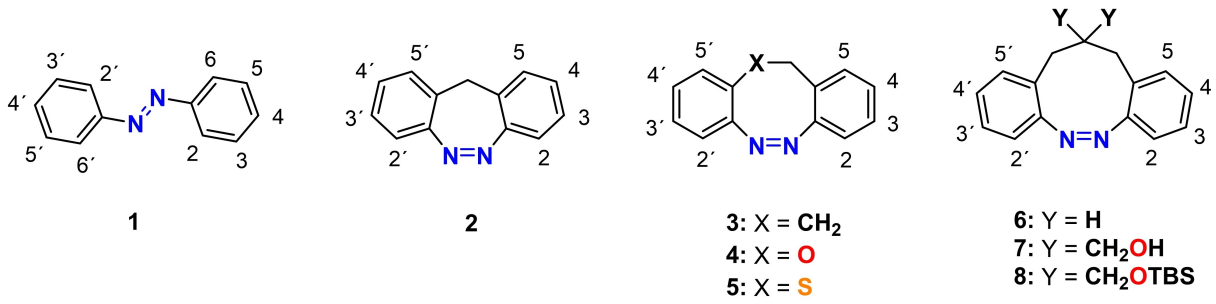

Scheme 1. Structures of the investigated compounds.

tives, we investigated azo derivatives **1**–**8** (Scheme 1) based on their redox potentials, absorption spectra, geometry, and the electronic structures of the resulting radical anions. The corresponding spectroscopic and calculated data will provide a systematic basis to evaluate the reduction-induced configurational isomerization (topology) in bridged derivatives **2**–**8**.

Results and Discussion

Redox Potentials

Generally, azo compounds exhibit at least two consecutive one-electron reductions producing a radical anion, and subsequently a dianion (Figure S1).[41] Whereas the first electron transfer is essentially reversible, this is not the case for the second. For the isomerizations discussed here only the first step leading to radical anions is relevant.

Standard cyclic voltammetry (with 0.1–1 Vs^{-1} scan rates) of *E*- and *Z*- azobenzene (**1**) shows matching cyclic voltammograms (CV). Starting with either *E*- or *Z*-**1**, one electron reduction leads to the radical anion *E*-**1**$^{\bullet-}$, which is subsequently oxidized to the parent *E*-**1**. The E_{pc}–E_{pa} peak separation for the first reduction process of *E*-**1** is 70 mV. The use of fast scan rates (2–1000 Vs^{-1}) and photo modulated voltammetry (PMW), allowed for the observation of *Z*-**1**$^{\bullet-}$, and indicate that *Z*-**1** is reduced at slightly more negative potential (60 mV, shifted in cathodic direction) than the *E* isomer. Furthermore, *Z*-**1**$^{\bullet-}$ rapidly converts to *E*-**1**$^{\bullet-}$ in a catalytic cycle, producing *E*-**1** upon re-oxidation. Consequently, the E_{pc}–E_{pa} peak separation is slightly larger for *Z*-**1**,[42] and PMW indicated a slight solvent dependence of the reduction potentials in organic solvents.[43]

We have performed CV experiments for the bridged azo derivatives **2**–**8**, all of which exist as *Z* isomers in their parent form with *E*-**1** serving as the reference (Table 1. Figure S1). The reduction peak potentials, E_{pc}, of **2**–**8** in the *Z* form range between −1,51 and −1.77 V vs. Fc^+/Fc (Table 1). These values are clearly less negative than those of parent *Z*-**1** (−1.94 V vs. Fc^+/Fc). Furthermore, the *Z*-derivatives of **2**–**8** show large E_{pc}–E_{pa} peak separations (270-780 mV, Table 1). CV experiments with three consecutive cycles, indicated shifted curves after each run (Figure S2). We ascribe this to a chemical follow-up reaction of the *Z*-type radical anions **2**$^{\bullet-}$–**8**$^{\bullet-}$. Based on the substantial negative charge at the N=N moiety (mirrored by the ^{14}N hyperfine couplings, described in the EPR section below), the *Z*-type radical anions of **2**–**8** act as strong (electrogenerated) bases. Such bases (A$^{\bullet-}$) tend to disproportionate yielding the neutral parent compound (**A**) and the corresponding dianion (**A**$^{2-}$).[44,45] The latter then reacts with protic impurities in DMF, forming the mono-protonated dianion (H**A**$^-$), which is further protonated to hydrazine derivative (H_2**A**, Scheme 2). In addition, a nucleophilic attack of the monoprotonated dianion (H**A**$^-$) onto DMF is likely, forming an additional redox-active species. These latter products are oxidized at much less negative potentials (with E_{pa} - E_{pc} peak separations of 100–700 mV[46–50] compatible with the data in Table 1 (270–780 mV)). Such a reactivity has been thoroughly established for a series of azobenzene derivatives with restricted conformational freedom embedded in monolayers.[49–53]

We have also followed the electrochemical reduction of the thermodynamically less stable *E* isomers of **3**–**8** (an *E* isomer of **2** could not be verified). To that end, solutions of **3**–**8** in DMF with electrolyte present, were irradiated with high power light

Table 1. Electrochemical data for **1**–**8** (scan rate 300 mVs^{-1}; solvent, degassed DMF; supporting electrolyte 0.1 $mol\,L^{-1}$ $TBAClO_4$; pseudo reference electrode, Ag wire; counter electrode and working electrode Pt (for **7**, and **8**, Au wire); potentials are referenced to Fc^+/Fc.

Compound	E_{pc}/V	E_{pa}/V	(E_{pc}–E_{pa})/mV
E-**1**[a]	−1.82	−1.75	70
E-**1**	−1.88[b]	−1.79[c]	70[d]
Z-**1**	−1.94[e]		
2	−1.69	−1.07	620
3	−1.68	−1.05	630
4	−1.74	−0.98	760
5	−1.66	−0.91	750
Z-**6**	−1.77	−0.99	780
E-**6**	−2.07	−1.94	130
Z-**7**	−1.61	−1.09	520
E-**7**	−1.99	−1.93	60
Z-**8**	−1.51	−1.24	270
E-**8**	−1.93	−1.87	60

[a] This work; [b] The value of −1.88 V vs Fc/Fc^+ was obtained by recalculating the literature value of −1.39 V vs SCE (in DMF)[57] from polarographic measurements; [c] The value of −1.79 V vs Fc/Fc^+ was obtained by recalculating the literature value of −1.32 V vs SCE (in DMF)[57] from polarographic measurements; [d] The value of 70 mV was obtained by taking $|E_{pc}–E_{pa}| = (1.39\,V–1.32\,V)$;[57] [e] The value of −1.94 V vs Fc/Fc^+ was obtained by recalculating the literature value of −1.40 V −0.060 V vs SCE.[42]

© 2023 The Authors. Chemistry - A European Journal published by Wiley-VCH GmbH

15213765, 2023, 35, Downloaded from https://chemistry-europe.onlinelibrary.wiley.com/doi/10.1002/chem.202300146 by CochraneAustria, Wiley Online Library on [22/08/2023]. See the Terms and Conditions (https://onlinelibrary.wiley.com/terms-and-conditions) on Wiley Online Library for rules of use; OA articles are governed by the applicable Creative Commons License

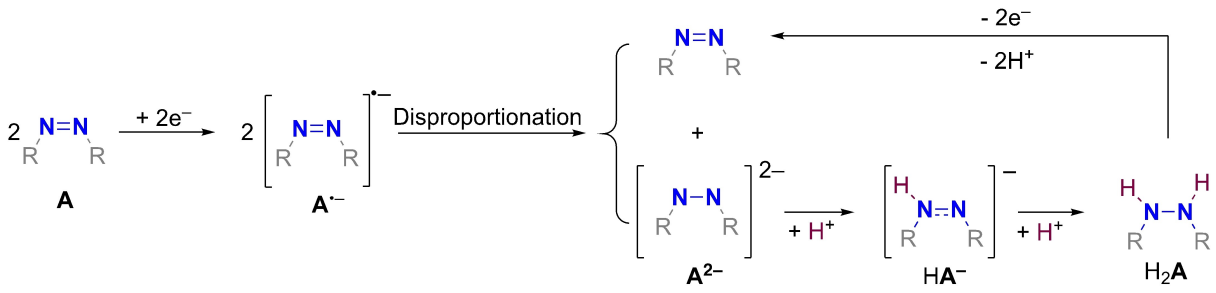

Scheme 2. The (electro)chemical behavior of azo compounds upon one electron reduction.

emitting diodes (LEDs, at appropriate wavelengths) until a photo stationary state (PSS) was accomplished. The amount of the *E* isomer in the PSS depends on the quantum yield of isomerization and the irradiation wavelength. For **3**–**8**, a *ca.* 70–90% enrichment of the *E* isomer can be achieved. However, the thermal half-life of *E*-**4** ($t_{1/2}$ = 89 s @ 20 °C) is too short to allow recording CVs attributable to the *E* isomer. In the case of *Z*-**3** ($t_{1/2}$ = 4.5 h @ 29 °C) and *Z*-**5** ($t_{1/2}$ = 3.5 d @ 27 °C)[54,55] the respective *E* isomers are thermally stable enough for electrochemical measurements. The CVs for *E*-**3** and *E*-**5** are identical to those of the corresponding *Z* isomers. This observation points to a similar behavior for *E*-**3**(*E*-**5**) as observed for *Z*-**1**. That is, *E*-**3**(*E*-**5**) upon reduction produce *E*-**3**$^{\bullet-}$(*E*-**5**$^{\bullet-}$), which rapidly isomerize to the corresponding *Z*$^{\bullet-}$ isomers. This can be traced back to the lower energy barrier for the *E*→*Z* isomerization in the radical anion (an anti-bonding π orbital is occupied weakening the N=N bond) compared with the neutral species and the relatively flexible diazocine skeleton. Furthermore, Z-**3**$^{\bullet-}$(*Z*-**5**$^{\bullet-}$) undergo a further chemical reaction (once again due to the high spin density at the nitrogen atoms) to the monoprotonated dianion and/or hydrazine derivatives, which are subsequently oxidized allowing for the formation of parent *Z*-**3**(*Z*-**5**) (in analogy to the CVs starting with pure *Z*-**3**(*Z*-**5**)).

Diazonine derivatives **6**–**8**, comprising trimethylene bridge, however, reveal a remarkable behavior: *E* and *Z* isomers provide clearly distinct CVs (Figure 1). For the parent *Z* isomer of compound **6** (black curve in Fig 1a) we observed a broad reduction peak, E_{pc}, at −1.77 V (vs. Fc^+/Fc) with a re-oxidation at −0.99 V presenting a large (E_{pc} - E_{pa}) separation of 780 mV. Upon irradiation with 405 nm LED of the freshly prepared solution of **6**, we reached PSS with *Z*/*E* ratio of 1:3 (*E*-**6**, $t_{1/2}$ > 2 weeks[54]), the CV of this solution showed an additional reduction (E_{pc} = −2.07 V accompanied with E_{pa} = −1.94 V, vs. Fc^+/Fc, E_{pc}−E_{pa} = 130 mV). We attribute this peak to the *E* isomer (Figure 1a and Table 1). This assignment is based on the findings from an investigation on related crown-ether-bridged azobenzenes, where it was shown that geometries resembling the *Z* configuration have anodically shifted E_{pc} values vs. *E* isomers.[56] DFT calculations provide an explanation for the observation of two distinct radical anions *E*- and *Z*-**6**$^{\bullet-}$. A saddle-point search for the *E*/*Z* isomerization of **6**$^{\bullet-}$ yielded a transition state with one imaginary frequency being 60 kJmol^{-1} higher in energy than *E*-**6**$^{\bullet-}$ (Figure S5). The much smaller (E_{pc} - E_{pa}) separation for the *E*-isomer is in line with a more extended electron delocalization into phenyl rings for *E*-**6**$^{\bullet-}$ than for *Z*-**6**$^{\bullet-}$ (*cf.* DFT calculations, Figure S33). Accordingly, the excess of the negative charge at N=N moiety diminishes. Consequently, the *E*-type radical anions are less basic than their *Z*-type counterparts and the reaction sequence shown in Scheme 2 is not observable. This is substantiated by a multi-cycle CV experiment lacking the potential shifts detected for the *Z*-derivatives (Figure S6).

Diazonines **7** and **8** display a redox behavior related to that of **6** for their *E* and *Z* isomers (Figure 1b and c, Table 1, and

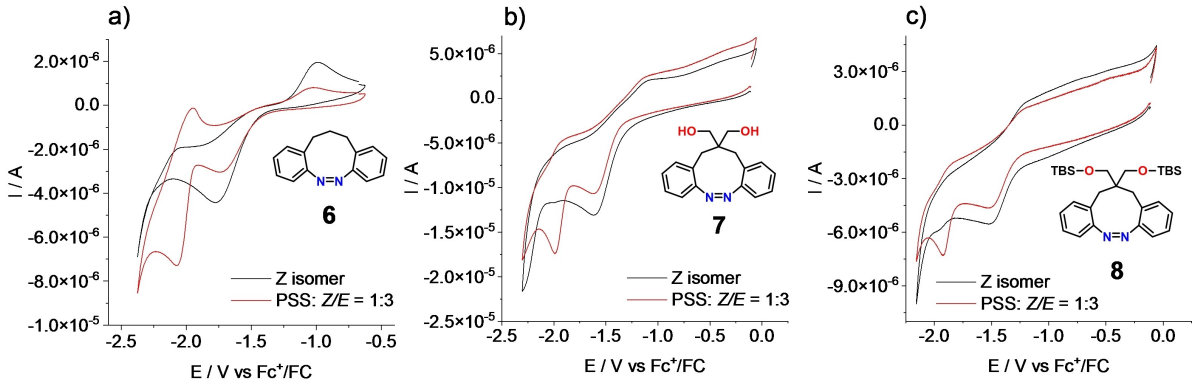

Figure 1. Cyclic voltammograms of a) *E* and *Z*-**6** b) *E* and *Z*-**7**, c) *E* and *Z*-**8** (scan rate, 300 mVs^{-1} solvent, degassed DMF; supporting electrolyte 0.1 mol L^{-1} $TBAClO_4$; a pseudo reference electrode, Ag wire; counter electrode and working electrode Pt (for **7**, and **8**, Au wire); potentials are referenced to Fc^+/Fc.

© 2023 The Authors. Chemistry - A European Journal published by Wiley-VCH GmbH

15213765, 2023, 35, Downloaded from https://chemistry-europe.onlinelibrary.wiley.com/doi/10.1002/chem.202300146 by CochraneAustria, Wiley Online Library on [22/08/2023]. See the Terms and Conditions (https://onlinelibrary.wiley.com/terms-and-conditions) on Wiley Online Library for rules of use; OA articles are governed by the applicable Creative Commons License

Figure S3 and S4). In the case of **7** the two hydroxy protons lead to additional peaks (Figure S4) likely connected with follow-up reactions of the primary radical anion of *E*/*Z*-**7**. The electron withdrawing groups CH_2OTBS lead to the slightly more positive E_{pc} values for **8**. The characteristic feature of diazonines **6**–**8** is their persistence vs. *Z*↔*E* isomerization upon one-electron reduction.

Spectroelectrochemistry

Our in-house built spectroelectrochemical cell allows us to couple irradiation, UV-Vis spectroscopy, and cyclic voltammetry enabling the observation of in-situ UV-Vis spectra during the potential controlled electrolysis (Figure S7).

As established by the CV experiments, *E* isomers of **3**–**5** rapidly convert to their *Z* isomers upon reduction. Correspondingly only the *Z* isomers of those compounds could be subjected to potential controlled electrolysis. To that end, *Z*-**2**-**5** were reduced under potential controlled conditions (applied potential is kept constant through the experiment), while following the temporal changes in the absorption spectra. Derivative *Z*-**2** did not show any change in the absorption spectra up to the maximum applied potential of −1.90 V (vs. Fc^+/Fc). *Z*-isomers of **3**–**5** were reduced to their radical anions by applying potentials being 40–90 mV more positive vs. the corresponding E_{pc} values (Table 1). The reduction time was adjusted to prevent the buildup of undesired side products. The results are presented in Figure 2 and the curves below the optical spectra indicate the temporal change of the absorbance for the bands at the wavelengths marked in the spectra. Diazocine derivatives **3**–**5** show new bands above 450 nm, which can be attributed to the corresponding radical anions based on similarity with previously reported spectra for the reduction of azobenzene derivatives.[40,58] For *Z*-**4** a potential of −1.70 V (vs. Fc^+/Fc) was applied to observe the newly formed bands with maxima at 470 nm and 500 nm. For compounds *Z*-**3** and *Z*-**5** a potential of −1.60 V (vs. Fc^+/Fc) was sufficient to obtain spectra showing the long-wavelength absorptions (Figure 2).

For diazonine *Z*-**6** applying −1.60 V (vs. Fc^+/Fc) leads to the appearance of a new absorption band at 523 nm, which is attributable to radical anion *Z*-$\mathbf{6}^{\bullet-}$ (Figure 3a, see also below). After electrolysis, the characteristic band of *Z*-**6** remains unchanged (black and red curve in Figure 3a). This is borne out by ^{1}H NMR analysis of the reaction mixture before/after the spectroelectrochemical experiment (potential-controlled reduction), which reveals no new peaks that could be attributed to *E*-**6** thus excluding *Z*→*E* isomerization via the radical anion (Figure S8). Irradiating parent *Z*-**6** at 405 nm (high power LED) leads to a 75% enrichment of *E*-**6** in solution (PSS). For control, we have performed a ^{1}H NMR analysis of the PSS in DMF in the presence of the supporting electrolyte (0.1 mol L^{-1} $TBAClO_4$) to exclude that the solution used for the spectroelectrochemical measurement already causes thermal isomerization. Even after letting the solution at room temperature for 24 h, the NMR spectrum was invariant (Figure S9). After performing the potential-controlled electrolysis on the PSS of **6** (*E*/*Z* = 3:1) the

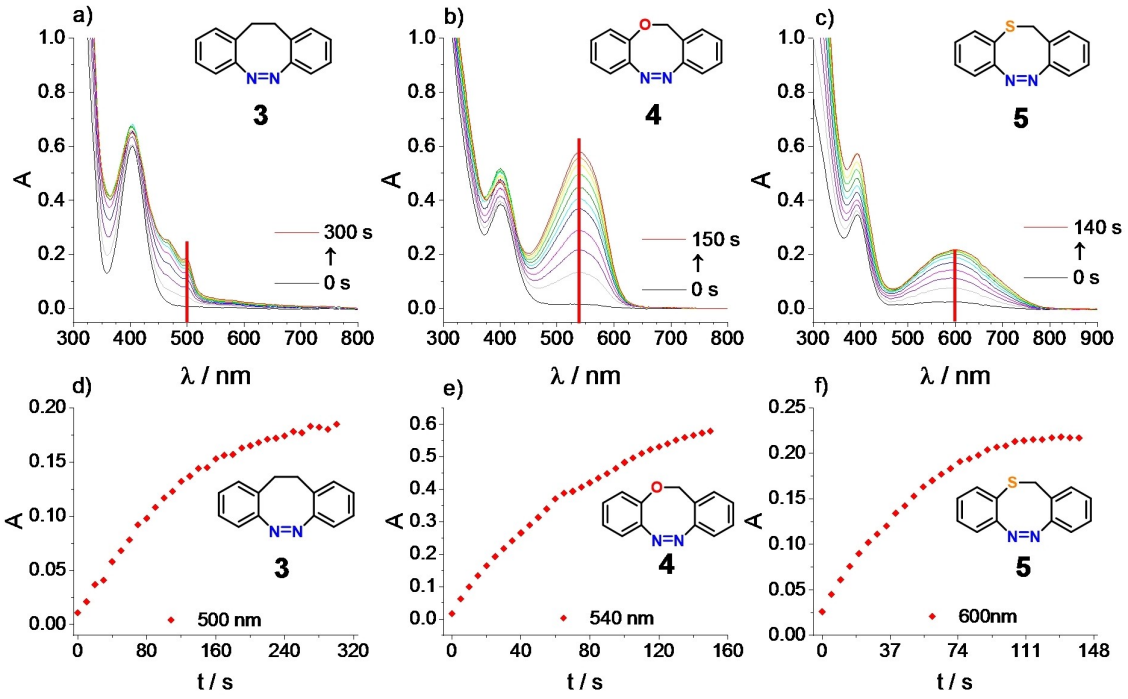

Figure 2. Potential controlled reduction of diazocine derivatives. a) reduction of *Z*-**3** by applying the potential of −1.60 V, b) reduction of *Z*-**4** by applying the potential of −1.70 V, c) reduction of *Z*-**5** by applying the potential of −1.60 V. The time profiles of the emerging bands are shown in d), e), and f). Potentials vs. Fc^+/Fc.

© 2023 The Authors. Chemistry - A European Journal published by Wiley-VCH GmbH

15213765, 2023, 35, Downloaded from https://chemistry-europe.onlinelibrary.wiley.com/doi/10.1002/chem.202300146 by CochraneAustria, Wiley Online Library on [22/08/2023]. See the Terms and Conditions (https://onlinelibrary.wiley.com/terms-and-conditions) on Wiley Online Library for rules of use; OA articles are governed by the applicable Creative Commons License

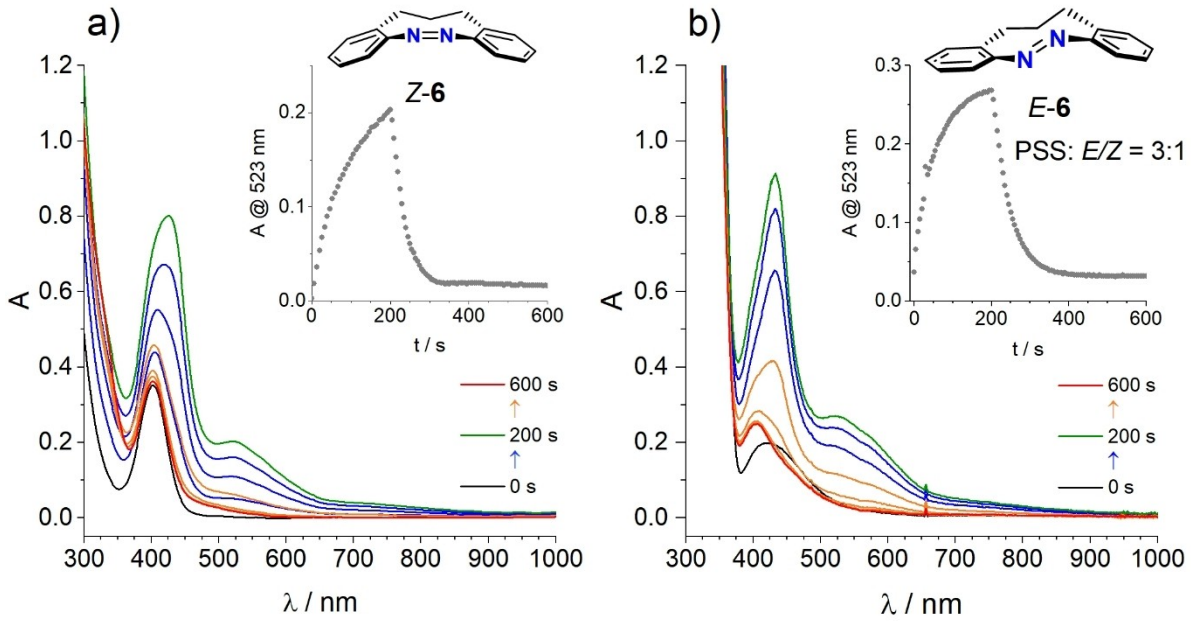

Figure 3. Potential controlled electrolysis a) of *Z*-**6** at a potential of −1.60 V (working electrode, vs Fc/Fc^+); b) of *E*-**6** (75 % in the PSS) with −1.80 V (working electrode, vs Fc/Fc^+). Inserts at a) and b) show the corresponding time profiles of the absorbance at 523 nm. In both cases, the electrochemical cell was disconnected after t = 200 s.

UV-vis spectra show only minimal conversion of *E*-**6** to *Z*-**6** indicated by a weak band emerging at 405 nm (red curve in Figure 3b). This observation is substantiated by the ^{1}H NMR analysis, which showed basically unchanged NMR signals and signal intensities after electrolysis (Figure S10 and S11). When the potential was turned off (after 200 s, physical disconnection of the electrodes via relay from the potentiostat), for both, the *Z* and the *E* isomer the band at 523 nm decayed within *ca.* 100 s indicating the short lifetime of the radical anions under our experimental conditions.

Derivative **7** with two alcoholic OH groups at the central position of the trimethylene bridge undergoes a proton transfer at the stage of the radical anion thus impairing further potential controlled electrolysis experiments (see Figure S12). However, compound *E*/*Z*-**8** having tert-butyldimethylsilyl (TBS) substituents resembles the reactivity described above for **6** (see Figure S13).

Another test for the unique behavior of *Z*-**6** is provided by redox cycling. We have performed an experiment, in which the potential alternates between −1.60 V (reduction of *Z*-**6**) and −1.20 V (value chosen to be lower than E_{pa} of *Z*-**6**, that is lower than the oxidation potential of **6**-H) while simultaneously monitoring the UV-Vis spectrum of the solution. The time for the reduction and the oxidation steps was arbitrarily chosen to be 2.5 min. Figure 4a shows a contour plot of the UV-vis spectra vs. time (the voltage vs. time profile is presented on the left side of the graph) indicating the decomposition of *Z*-**6**. This can be additionally substantiated from Figure 4b, showing the UV-vis spectra at the end of every reduction cycle, once again indicating the decomposition of *Z*-$\mathbf{6}^{\bullet-}$ with every consecutive cycle, insert in the Figure 4b shows the absorbance at 523 nm vs. time, correlated to the cycling potential. Using LC–MS data obtained from the reaction solutions, we have identified hydrazine **6**-H (Scheme 3) as the main product, providing further evidence about the hydrazine **6**-H as the dominant species in the overall redox process of *Z*-**6**. This observation is in line with CV experiments and the previously reported electrochemical behavior of azo compounds.[41,58,59] However we could not establish any traces revealing that *E*-**6** is converted to its *Z* isomer via one-electron reduction (Scheme 3, red arrow).[57,60]

EPR spectroscopy

The radical anions of **1**, **2**, **3**, and **6** have already been reported many years ago,[14,22,27,29] however, their formation via *E* or *Z* precursors and the connection of the radical anions to redox potentials and optical spectra is elusive. We have, therefore, included these derivatives into our discussion (the corresponding spectra are presented in the Supporting Information). Selected EPR data of radical anions generated from **1**–**6** and **8** is presented in Table 2.

The EPR spectra of radical anions derived from azo compounds are essentially dominated by a 1:2:3:2:1 quintet pattern produced by the two equivalent ^{14}N nuclei (Figure 5) except **4** and **5**, where the two nitrogen nuclei are inequivalent (see Table 2). This is caused by the highly dominating part of the spin population residing at the N=N moiety. ^{1}H isotropic hyperfine coupling constants (hfcs) attributed to the aromatic substituents provide additional information on the electron delocalization and topology of anions $\mathbf{1}^{\bullet-}$–$\mathbf{6}^{\bullet-}$ and $\mathbf{8}^{\bullet-}$.

© 2023 The Authors. Chemistry - A European Journal published by Wiley-VCH GmbH

15213765, 2023, 35, Downloaded from https://chemistry-europe.onlinelibrary.wiley.com/doi/10.1002/chem.202300146 by CochraneAustria, Wiley Online Library on [22/08/2023]. See the Terms and Conditions (https://onlinelibrary.wiley.com/terms-and-conditions) on Wiley Online Library for rules of use; OA articles are governed by the applicable Creative Commons License

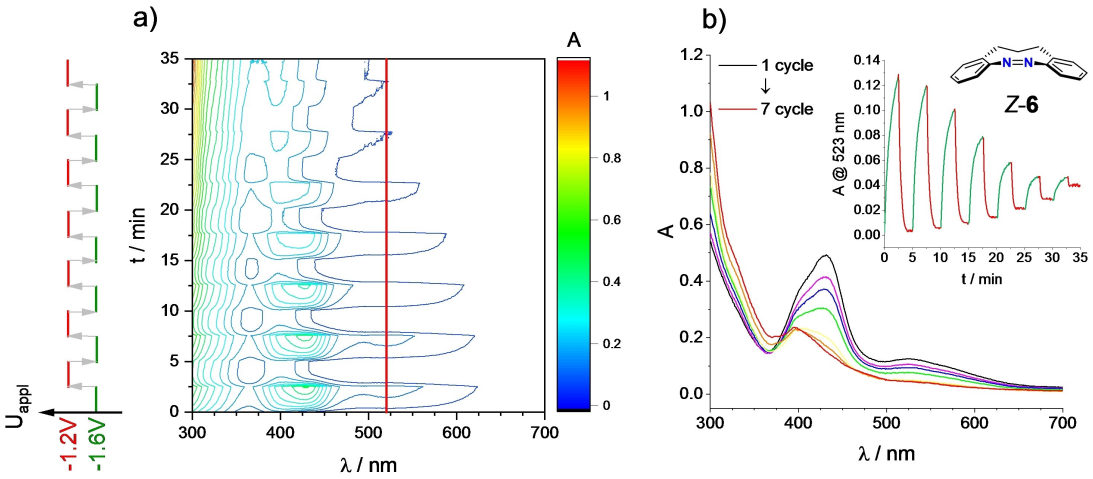

Figure 4. Potential toggling experiment of *Z*-**6**. a) UV-vis spectrum vs. time presented as a contour graph, with a legend on the left side indicating the time profile of the toggling potential. b) UV-vis spectra of the reaction mixture at seven points during the experiment, each point representing the final time for the reduction part of the overall cycle. Insert shows absorbance at 523 nm vs. time.

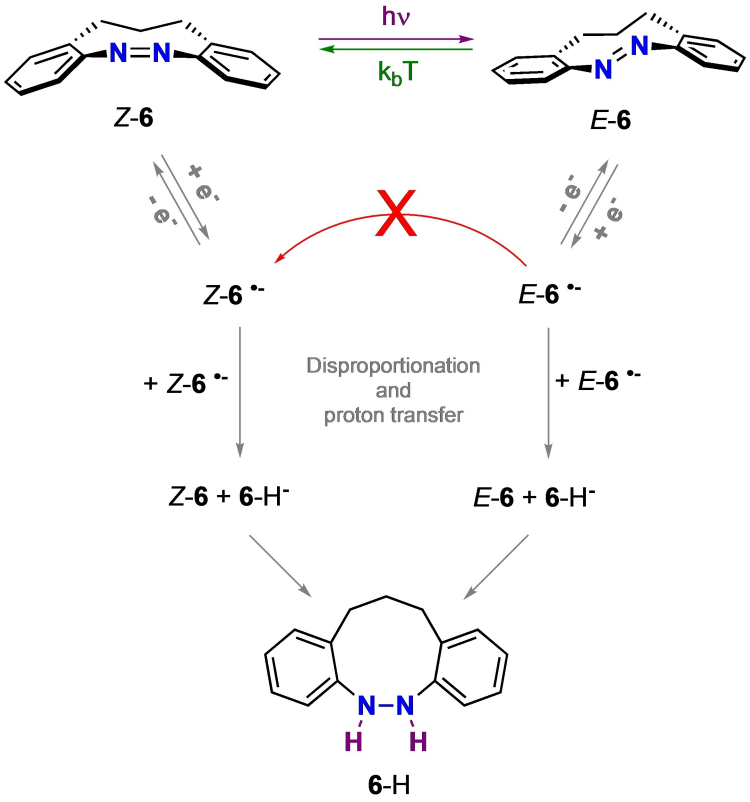

Scheme 3. Electrochemical reduction of *E*/*Z*-**6** and the formation of **6**-H by protic impurities.

Previous publications reveal that the radical anions of aromatic but also those of aliphatic azo compounds are π-type radicals and the variations of the ^{14}N hfcs reflect the amount of the spin residing at the N=N π system. Accordingly, the higher the ^{14}N hfc the more the charge and the spin are confined to the azo moiety.

The radical anion of parent azobenzene, *E*-**1**$^{\bullet-}$, reveals a ^{14}N hfc of *ca.* 0.5 mT and the highest ^{1}H hfc attributable to the aromatic protons in the 4,4′ positions (*ortho*) in the phenyl substituents amounts to 0.32 mT (Table 2). The ^{14}N hfcs and the ^{1}H hfcs assigned to the 4,4′ positions are additionally suitable candidates to monitor electron delocalization in **1**$^{\bullet-}$–**6**$^{\bullet-}$ and **8**$^{\bullet-}$. In **2**$^{\bullet-}$, the monomethylene bridge between the two

© 2023 The Authors. Chemistry - A European Journal published by Wiley-VCH GmbH

15213765, 2023, 35, Downloaded from https://chemistry-europe.onlinelibrary.wiley.com/doi/10.1002/chem.202300146 by CochraneAustria, Wiley Online Library on [22/08/2023]. See the Terms and Conditions (https://onlinelibrary.wiley.com/terms-and-conditions) on Wiley Online Library for rules of use; OA articles are governed by the applicable Creative Commons License

15213765, 2023, 35, Downloaded from https://chemistry-europe.onlinelibrary.wiley.com/doi/10.1002/chem.202300146 by CochraneAustria, Wiley Online Library on [22/08/2023]. See the Terms and Conditions (https://onlinelibrary.wiley.com/terms-and-conditions) on Wiley Online Library for rules of use; OA articles are governed by the applicable Creative Commons License

Table 2. EPR data for radical anions **1**$^{\bullet-}$–**6**$^{\bullet-}$ and **8**$^{\bullet-}$, solvent THF, counterion K^+ (the data reflect the values used for the simulations of the EPR spectra and are based on ENDOR measurements together with DFT calculations for the assignments, see Supporting Information, errors ≤10%).

Radical anion	g factor[b]	^{14}N hfc/mT	^{1}H hfc/mT 2,2′	3,3′	4,4′	5,5′	6,6′	CH_2
1$^{\bullet-}$[a]	-	0.478 (2 N)	0.211	0.062	0.320	0.089	0.294	
2$^{\bullet-}$[a]	2.0037	0.654 (2 N)	0.234	0.083	0,305	0.132	–	0.132
3$^{\bullet-}$[a]	2.0041	0.927 (2 N)	0.098	0.065	0.113	0.076	-	0.154
4$^{\bullet-}$[c]	2.0039	0.967/0.850	0.035	0.065	0.004	0.183		0.014
				0.001	0.245	0.150		0.319
5$^{\bullet-}$	2.0037	0.567/0.485	0.279	0.141	0.220	0.141		0.316
6$^{\bullet-}$	2.0036	0.969 (2 N)	0.184	0.114	0.220	0.114		0.196
								0.013
8$^{\bullet-}$		0.969 (2 N)						

[a] Values are in agreement with those reported in the Ref. [29,11]. Signs are omitted. [b] Exp. error: ±0.0002. [c] Assignments based on calculations, see Supporting Information.

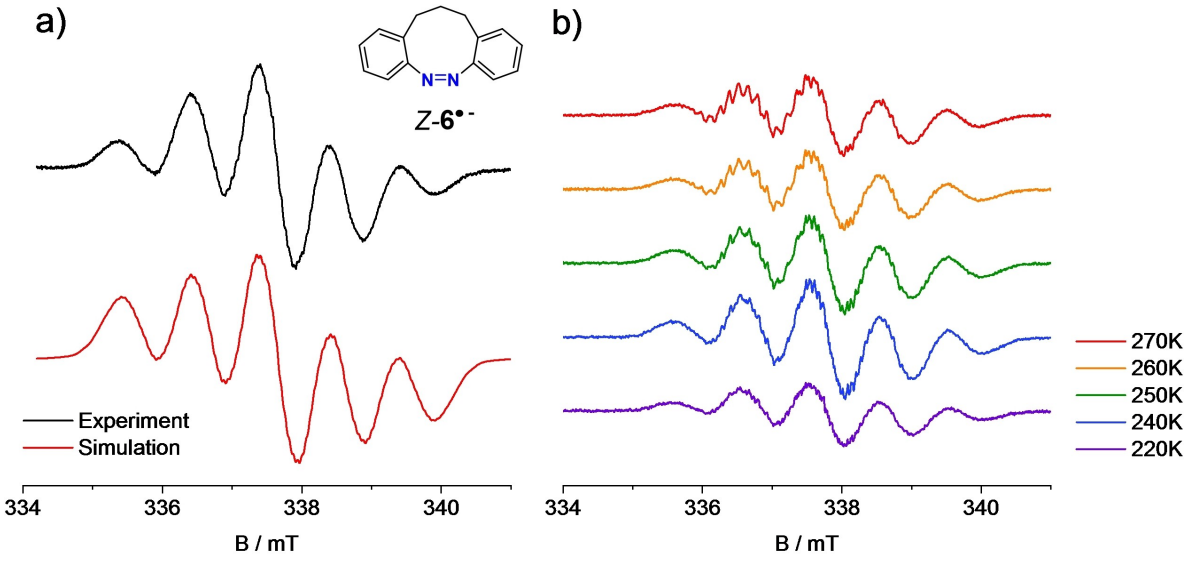

Figure 5. EPR spectra of **6**$^{\bullet-}$ a) experimental spectra recorded at 200 K together with simulation, b) experimental spectra at temperature from 220 K to 270 K.

benzene rings only allows a slightly bent *Z*-type arrangement of the azobenzene moiety impairing electron delocalization toward the benzene rings. Accordingly, the ^{14}N hfc rises (vs. *E*-**1**$^{\bullet-}$) to 0.654 mT whereas the *ortho* ^{1}H hfc decreases to 0.305 mT mirroring a higher spin population at the nitrogen atoms with an attenuated delocalization into the benzene rings. Parent diazocine and diazonine radical anions **3**$^{\bullet-}$ and **6**$^{\bullet-}$ reveal significantly higher, rather similar ^{14}N hfcs of 0.927 and 0.969 mT, respectively, and, in parallel, smaller ^{1}H hfcs for the 4,4′ hydrogens. These data closely resemble those of alkyl azo derivatives **9**$^{\bullet-}$–**11**$^{\bullet-}$[22,27,28,38] having ^{14}N hfcs between *ca.* 0.8 and 1 mT. This provides evidence that in **3**$^{\bullet-}$ and **6**$^{\bullet-}$ the spin and the charge are confined to the central azo moiety (π-type radicals) and is in very good agreement with our DFT calculations (Figure 6a and b, see Figure S33).

Derivative **5**$^{\bullet-}$ reveals rather small ^{14}N hfcs of 0.567 and 0.485 mT (two non-equivalent nitrogen nuclei in **5**$^{\bullet-}$, Table 3). Both values are close to that of azobenzene radical anion **1**$^{\bullet-}$ and to **2**$^{\bullet-}$ where the aromatic π systems are essentially coplanar to the N=N moiety and a substantial portion of the spin is delocalized onto the benzene rings. Accordingly, **5**$^{\bullet-}$ must adopt a topology substantially differing from the related (central diazocine ring) derivatives **3**$^{\bullet-}$ and **4**$^{\bullet-}$ possessing

Table 3. Experimental (by simulation, ^{14}N ENDOR not detectable) and calculated ^{14}N hfcs/mT for **1**$^{\bullet-}$–**6**$^{\bullet-}$ and **8**$^{\bullet-}$–**11**$^{\bullet-}$ (counterion, K^+) together with the assignment to geometries (see Figure 7) based on b3lyp/6-31g(d) calculations. The calculated data with the best match with the experimental values are in italics.

Radical anion	Exp. ^{14}N hfc	Configuration/Conformation and Calc. ^{14}N hfc		
		Z	*E1*[a]	*E2*[a]
1$^{\bullet-}$	0.478 (2 N)			
2$^{\bullet-}$	0.654 (2 N)	*0.63*	1.60	
3$^{\bullet-}$	0.927 (2 N)	*1.02*	1.25	
4$^{\bullet-}$	0.967/0.850	*0.97/0.99*	1.38/1.42	
5$^{\bullet-}$	0.567/0.485	1.09/1.08	*0.82/0.58*	1.40/1.40
6$^{\bullet-}$(**8**$^{\bullet-}$)	0.969 (2 N)	*0.97*	0.56	1.16
9$^{\bullet-}$	0.918 (2 N)			
10$^{\bullet-}$	0.878 (2 N)			
11$^{\bullet-}$	0.80 (2 N)			

[a] *E1*/*E2* applies to diazocine **5**, see text.

© 2023 The Authors. Chemistry - A European Journal published by Wiley-VCH GmbH

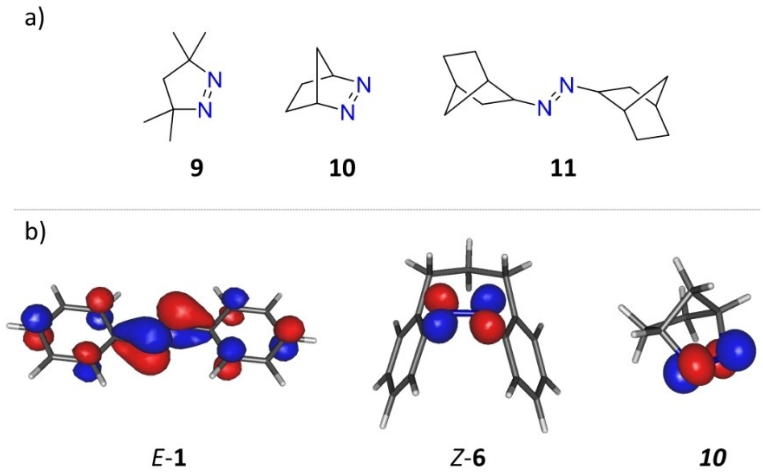

Figure 6. a) Structures of alkyl azo derivatives **9**–**11**, b) Selected LUMOs of **1**, **6**, **10** (see the Supporting Information for the remaining derivatives.[61]

clearly higher ^{14}N hfcs (0.927 and 0.967/0.850, respectively). This is borne out by DFT calculations, predicting the smallest ^{14}N hfcs for a *E*1 configuration of **5**$^{\bullet-}$ (Figure 7). The calculated ^{14}N data, in this case are not as well matching with the experiment as those for the remaining derivatives; nevertheless, the predictions are clearly substantially smaller than for a *Z* or *E*2 configurations of **5**$^{\bullet-}$ and using bigger ^{14}N hfcs for the spectral simulation does not produce any match with the experimental spectrum.

Diazonine derivatives **6**$^{\bullet-}$–**8**$^{\bullet-}$ have shown remarkable cyclovoltammograms (Figure 1) implying that the *Z* and *E* topology in the parent compounds is retained upon reduction. Unfortunately, the reduction potential of the *Z* isomer is less negative than that of the *E* isomer (−1.77 vs. −2.07 V vs. Fc^+/Fc) and *Z*-**6** is always a well distinguishable component of the PSS (*Z*/*E* = 1 : 3, see Supporting Information). Accordingly, the *Z* isomer is preferentially reduced via K-metal before *E*-**6** is reduced. This leads to *Z*-**6**$^{\bullet-}$ being the dominating component of the EPR spectra with *E*-**6**$^{\bullet-}$ remaining indistinguishable.

The UV-Vis spectra taken from the EPR samples resemble those assigned to the radical anions based on the investigations by spectroelectrochemistry.

Overall Considerations

In general, this investigation of the bridged azobenzenes **2**–**8** has shown, that one-electron reduction of the parent compounds yields radical anions with well-distinguishable geometries and electronic structures. The combination of EPR data, one-electron reduction potentials ((spectro)electrochemistry), optical spectra, and DFT calculations reveals rather specific geometry changes when going from the parent neutral azo derivatives to the radical anions. The character of the bridging

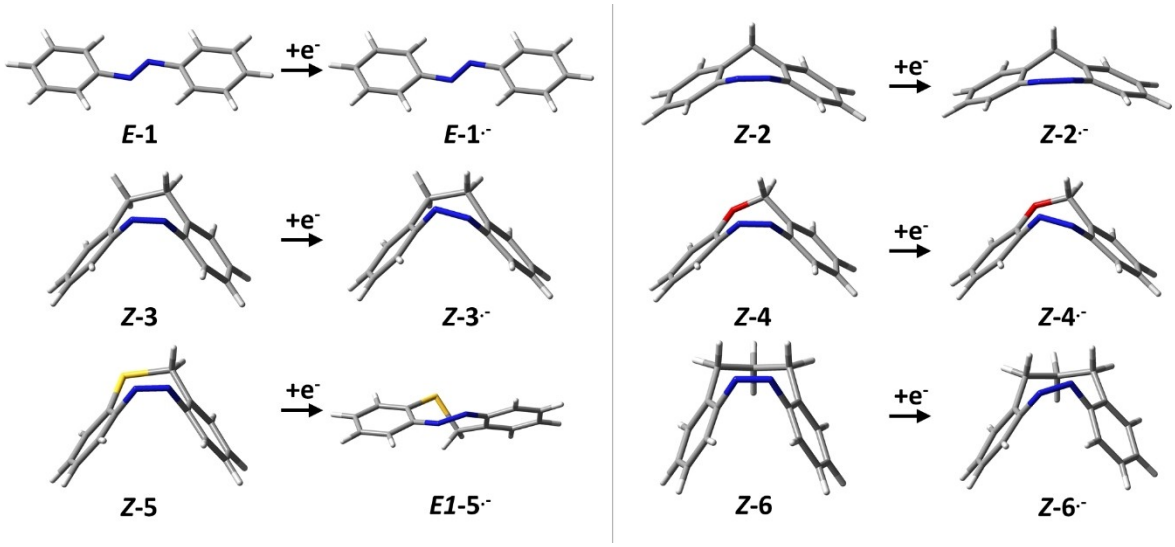

Figure 7. Calculated geometries of **3**$^{\bullet-}$–**6**$^{\bullet-}$.

© 2023 The Authors. Chemistry - A European Journal published by Wiley-VCH GmbH

15213765, 2023, 35, Downloaded from https://chemistry-europe.onlinelibrary.wiley.com/doi/10.1002/chem.202300146 by CochraneAustria, Wiley Online Library on [22/08/2023]. See the Terms and Conditions (https://onlinelibrary.wiley.com/terms-and-conditions) on Wiley Online Library for rules of use; OA articles are governed by the applicable Creative Commons License

15213765, 2023, 35, Downloaded from https://chemistry-europe.onlinelibrary.wiley.com/doi/10.1002/chem.202300146 by CochraneAustria, Wiley Online Library on [22/08/2023]. See the Terms and Conditions (https://onlinelibrary.wiley.com/terms-and-conditions) on Wiley Online Library for rules of use; OA articles are governed by the applicable Creative Commons License

units and the corresponding conformational flexibility of the central rings have a substantial influence on the redox potentials, charge distribution, reactivity (protonation) and the topology of the radical anions $\mathbf{1}^{\bullet-}$–$\mathbf{8}^{\bullet-}$. Whereas parent azobenzene **1** has been shown to rapidly form its thermodynamically preferred *E*-$\mathbf{1}^{\bullet-}$ isomer and the relatively rigid derivative **2** only slightly planarizes upon reduction, derivatives $\mathbf{3}^{\bullet-}$ and $\mathbf{4}^{\bullet-}$ retain a *Z*-type topology of the azo moiety, in which the spin and the charge are mainly concentrated at the azo π* orbitals. In the case of $\mathbf{5}^{\bullet-}$ the experimental parameters indicate a more planar *E*-type topology allowing substantial delocalization of the spin and the charge into the benzene rings. For **5**, there is an additional interplay of two *E* conformers (*E*1 and *E*2)[15] being populated in the parent state and the two conformations are translated into the radical anion, $\mathbf{5}^{\bullet-}$. Diazonines **6**–**8** reveal a particularly noteworthy feature: In contrast to the other derivatives, one-electron reduction does not lead to *E*/*Z* isomerization.

*E*xperimental Section

Cyclovoltammetry

Cyclovoltammetry measurements of azobenzene derivatives **1**–**8** was performed on an Autolab PGSTAT12 potentiostat (Eco Chemie BV, The Netherlands) connected to a PC running the software package Nova 2.1.4 (Metrohm, The Netherlands) in degassed DMF as a solvent containing 0.1 mol L^{-1} tetrabutylammonium perchlorate ($TBAClO_4$) as electrolyte employing Ag wire as a pseudo reference electrode, Pt wire as the counter electrode, and as a working electrode. the concentration of compounds **1–8** was at 1 mmol L^{-1} level, ferrocene was added to the solution after recording the CV of the compound and the measurement was repeated to reference the Ag electrode. The $E_{1/2}$ potential of ferrocene-ferrocenium couple was in good agreement with the literature value in all cases.[4]

Spectroelectrochemistry

The self-made spectroelectrochemical cell is constructed from machined PTFE with two CaF_2 optical windows separated by 6 mm and equipped with a three-electrode setup using Ag wire as pseudo reference electrode later referenced to Fc^+/Fc, Pt wire as a counter electrode, and Pt mesh electrode as the working electrode. The light path is perpendicular to the CaF_2 optical windows passing through the Pt mesh working electrode. Optical fibers are used to direct the light from the light source through the cell to the spectrometer (J&M Analytik AG, Essingen, Germany, UV-vis spectrometer equipped with 1024-pixel diode array detector, using stabilized Deuterium, and halogen lamp as the light source). In addition, the cell contains an inlet and outlet for liquid and can be sealed, thus permitting the measurements under oxygen-free conditions. Autolab PGSTAT12 potentiostat (Eco Chemie BV, The Netherlands), was used for the potential controlled electrolysis.

EPR Spectroscopy

Continuous-wave EPR spectra were recorded using a Bruker X-band spectrometer (EMX, 100 kHz field modulation) equipped with the temperature control unit (Eurotherm B-VT 2000). Typical conditions for spectra acquisition were: 2 mW of RF power and 0.1 mT field modulation amplitude. The compounds have been reduced to the corresponding radical anions using a potassium mirror in a tandem EPR cell under strict oxygen and water-free conditions. The tube was connected to the high vacuum line, after three cycles of evacuation, flame drying, and filling with argon one compartment was filled with the compound to be reduced. The potassium mirror was prepared by sublimation of potassium under high vacuum in another compartment. Followed by condensation of extra dry tetrahydrofuran (THF) to the compartment with the compound to be reduced. The solvent was degassed by three freeze and thaw cycles and the tube was sealed off. Shortly before measurement, the solution was cooled down and allowed to react with metallic potassium. The g factor was obtained using 2,2-Diphenyl-1-(2,4,6-trinitrophenyl)-hydrazyl (DPPH) in THF as external reference.

ENDOR Spectroscopy

The ENDOR spectra were recorded on a Bruker ESP 300 X-band spectrometer equipped with the temperature control unit (Eurotherm B-VT 2000).

DFT Calculations

All calculations were performed using the GAUSSIAN09 program package.[61] Using the B3LYP/tzvp protocol.[62,63] The geometries of the neutral compounds served as the starting point for calculating those of the corresponding radical anions. To account for solvation effects the conductor-like polarizable continuum model (cpcm)[64] was used to model THF, which is the solvent used for the samples for the EPR experiments (chemical reduction with K-metal in THF). It is known that calculations on N-centered radical anions at the B3LYP/tzvp level underestimate the ^{14}N hfc.[65] Therefore, the geometries of the radical anions were additionally optimized at the B3LYP/6-31g(d)[66] level, which produces higher values that fit the experimental data better. The energies and geometries for the isomers of **6** were taken from Ref. [67].

Acknowledgements

G.G. and G.G. thank NAWI Graz for support. R.H. is grateful for financial support from GRC667 'Function By Switching'. G. Gescheidt and K.K. thank the Porous Materials at Work for Sustainability (PMWS, TU Graz) for funding.

Conflict of Interests

The authors declare no conflict of interest.

Data Availability Statement

Research data are not shared.

Keywords: cyclic azobenzenes · EPR isomerization · one electron reduction · radical anions

[1] Z. L. Pianowski, *Chem. Eur. J.* **2019**, *25*, 5128–5144.
[2] A. H. Heindl, H. A. Wegner, *Chem. Eur. J.* **2020**, *26*, 13730–13737.

© 2023 The Authors. Chemistry - A European Journal published by Wiley-VCH GmbH

[3] H. Ren, P. Yang, F. M. Winnik, *Polymer. Chem.* **2020**, *11*, 5955–5961.
[4] A. I. Kovalchuk, Y. L. Kobzar, I. M. Tkachenko, Y. I. Kurioz, O. G. Tereshchenko, O. V. Shekera, V. G. Nazarenko, V. V. Shevchenko, *ACS Appl. Polym. Mater.* **2020**, *2*, 455–463.
[5] I. M. Welleman, M. W. H. Hoorens, B. Feringa, H. H. Boersma, W. Szymanski, *Chem. Sci.* **2020**, *11*, 11672–11691.
[6] J. Morstein, A. C. Impastato, D. Trauner, *ChemBioChem* **2021**, *22*, 73–83.
[7] J. Broichhagen, J. A. Frank, D. Trauner, *Acc. Chem. Res.* **2015**, *48*, 1947–1960.
[8] K. Hull, J. Morstein, D. Trauner, *Chem. Rev.* **2018**, *118*, 10710–10747.
[9] L. Heintze, D. Schmidt, T. Rodat, L. Witt, J. Ewert, M. Kriegs, R. Herges, C. Peifer, *Int. J. Mol. Sci.* **2020**, *21*.
[10] S. Venkataramani, U. Jana, M. Dommaschk, F. D. Sonnichsen, F. Tuczek, R. Herges, *Science* **2011**, *331*, 445–448.
[11] V. Wellm, J. Groebner, G. Heitmann, F. D. Sonnichsen, R. Herges, *Angew. Chem. Int. Ed.* **2021**, *60*, 8220–8226; *Angew. Chem.* **2021**, *133*, 8301–8307.
[12] V. Wellm, C. Nather, R. Herges, *J. Org. Chem.* **2021**, *86*, 9503–9514.
[13] E. Stadler, M. Dommaschk, P. Fruhwirt, R. Herges, G. Gescheidt, *ChemPhysChem* **2018**, *19*, 571–574.
[14] F. Gerson, A. Lamprecht, M. Scholz, D. Lenoir, *Helv. Chim. Acta* **1996**, *79*, 307–318.
[15] P. Lentes, J. Rudtke, T. Griebenow, R. Herges, *Beilstein J. Org. Chem.* **2021**, *17*, 1503–1508.
[16] A. L. Leistner, S. Kirchner, J. Karcher, T. Bantle, M. L. Schulte, P. Godtel, C. Fengler, Z. L. Pianowski, *Chem. Eur. J.* **2021**, *27*, 8094–8099.
[17] N. Eleya, S. Ghosh, E. Lork, A. Staubitz, *J. Mater. Chem.* **2021**, *9*, 82–87.
[18] M. S. Maier, K. Hüll, M. Reynders, B. S. Matsuura, P. Leippe, T. Ko, L. Schäffer, D. Trauner, *J. Am. Chem. Soc.* **2019**, *141*, 17295–17304.
[19] P. Lentes, E. Stadler, F. Rohricht, A. Brahms, J. Grobner, F. D. Sonnichsen, G. Gescheidt, R. Herges, *J. Am. Chem. Soc.* **2019**, *141*, 13592–13600.
[20] M. Hammerich, C. Schütt, C. Stähler, P. Lentes, F. Röhricht, R. Höppner, R. Herges, *J. Am. Chem. Soc.* **2016**, *138*, 13111–13114.
[21] F. Gerson, C. Sahin, *J. Chem. Soc. Perkin Trans. 2* **1997**, 1127–1132.
[22] R. J. Bushby, K. M. Ng, *J. Chem. Soc. Perkin Trans. 2* **1996**, 1053–1056.
[23] W. Adam, T. Kammel, *J. Org. Chem.* **1996**, *61*, 3172–3176.
[24] M. L. Greer, H. Sarker, M. E. Mendicino, S. C. Blackstock, *J. Am. Chem. Soc.* **1995**, *117*, 10460–10467.
[25] C. J. Rhodes, H. Agirbas, M. Lindgren, O. N. Antzutkin, *J. Chem. Soc. Perkin Trans. 2* **1993**, 2135–2139.
[26] G. Gescheidt, A. Lamprecht, J. Heinze, B. Schuler, M. Schmittel, S. Kiau, C. Rüchardt, *Helv. Chim. Acta* **1992**, *75*, 1607–1612.
[27] C. H. Ess, F. Gerson, W. Adam, *Helv. Chim. Acta* **1992**, *75*, 335–350.
[28] C. H. Ess, F. Gerson, *Helv. Chim. Acta* **1991**, *74*, 2078–2093.
[29] U. Buser, C. H. Ess, F. Gerson, *Magn. Reson. Chem.* **1991**, *29*, 721–725.
[30] P. S. Engel, W. X. Wu, *J. Am. Chem. Soc.* **1989**, *111*, 1830–1835.
[31] R. Sustmann, R. Sauer, *Chem. Commun.* **1985**, 1248–1249.
[32] U. Krynitz, F. Gerson, N. Wiberg, M. Veith, *Angew. Chem. Int. Ed.* **1969**, *8*, 755-&; *Angew. Chem.* **1969**, *81*, 745.
[33] U. Jung, J. Kubitschke, R. Herges, O. Magnussen, *Electrochim. Acta* **2013**, *112*, 869–880.
[34] F. L. Zhao, L. Grubert, S. Hecht, D. Bleger, *Chem. Commun.* **2017**, *53*, 3323–3326.
[35] C. Knie, M. Utecht, F. L. Zhao, H. Kulla, S. Kovalenko, A. M. Brouwer, P. Saalfrank, S. Hecht, D. Bleger, *Chem. Eur. J.* **2014**, *20*, 16492–16501.
[36] D. Bleger, J. Schwarz, A. M. Brouwer, S. Hecht, *J. Am. Chem. Soc.* **2012**, *134*, 20597–20600.
[37] A. Kitamura, N. Miyagawa, T. Karatsu, *J. Synth. Org. Chem. Jpn.* **1997**, *55*, 678–685.
[38] G. Gescheidt, A. Lamprecht, C. Rüchardt, M. Schmittel, *Helv. Chim. Acta* **1992**, *75*, 351–356.
[39] C. J. Saint-Louis, D. J. Warner, K. S. Keane, M. D. Kelley, C. M. Meyers, S. C. Blackstock, *J. Org. Chem.* **2021**.
[40] A. Goulet-Hanssens, M. Utecht, D. Mutruc, E. Titov, J. Schwarz, L. Grubert, D. Bléger, P. Saalfrank, S. Hecht, *J. Am. Chem. Soc.* **2017**, *139*, 335–341.
[41] G. H. Aylward, J. L. Garnett, J. H. Sharp, *Chem. Commun.* **1966**, 137–138.
[42] E. Laviron, E. L. Mugnier, *J. Electroanal. Chem.* **1978**, *93*, 69–73.
[43] G. Grampp, C. Muresanu, S. Landgraf, *J. Electroanal. Chem.* **2005**, *582*, 171–178.
[44] H. Lund, O. Hammerich, *Organic Electrochemistry*, 4 ed., Marcel Dekker (New York, Basel), **2001**.
[45] S. Cheng, M. D. Hawley, *J. Org. Chem.* **1985**, *50*, 3388–3392.
[46] H. Z. Yu, J. W. Zhao, Y. Q. Wang, Z. F. Liu, *Mol. Cryst. Liq. Cryst.* **1997**, *294*, 107.
[47] W. B. Caldwell, D. J. Campbell, K.-M. Chen, B. R. Herr, C. A. Mirkin, A. Malik, M. K. Durbin, P. Dutta, K. G. Huang, *J. Am. Chem. Soc.* **1995**, *117*, 6071.
[48] H. Z. Yu, Y. Q. Wang, J. Z. Cheng, J. W. Zhao, S. M. Cai, H. Inokuchi, A. Fujishima, Z. F. Liu, *Langmuir* **1996**, *12*, 2843.
[49] D. J. Campbell, B. R. Herr, J. C. Hulteen, R. P. Van Duyne, C. A. Mirkin, *J. Am. Chem. Soc.* **1996**, *118*, 10211–10219.
[50] B. R. Herr, C. A. Mirkin, *J. Am. Chem. Soc.* **1994**, *116*, 1157–1158.
[51] R. Wang, T. Iyoda, D. A. Tryk, K. Hashimoto, A. Fujishima, *Langmuir* **1997**, *13*, 4644–4651.
[52] H.-Z. Yu, S. Ye, H.-L. Zhang, K. Uosaki, Z.-F. Liu, *Langmuir* **2000**, *16*, 6948–6954.
[53] H.-Z. Yu, H.-L. Zhang, Z.-F. Liu, S. Ye, K. Uosaki, *Langmuir* **1998**, *14*, 619–624.
[54] P. Lentes, E. Stadler, F. Röhricht, A. Brahms, J. Gröbner, F. D. Sönnichsen, G. Gescheidt, R. Herges, *J. Am. Chem. Soc.* **2019**, *141*, 13592–13600.
[55] W. Moormann, T. Tellkamp, E. Stadler, F. Röhricht, C. Näther, R. Puttreddy, K. Rissanen, G. Gescheidt, R. Herges, *Angew. Chem. Int. Ed.* **2020**, *59*, 15081–15086; *Angew. Chem.* **2020**, *132*, 15193–15198.
[56] I. Zawisza, R. Bilewicz, E. Luboch, J. F. Biernat, *Supramol. Chem.* **1998**, *9*, 277–287.
[57] J. L. Sadler, A. J. Bard, *J. Am. Chem. Soc.* **1968**, *90*, 979–1989.
[58] K. G. Boto, F. G. Thomas, *Aust. J. Chem.* **1973**, *26*, 1251–1258.
[59] A. Kapturkiewicz, M. K. Kalinowski, *J. Phys. Chem.* **1978**, *82*, 1141–1144.
[60] P. Neta, H. Levanon, *J. Phys. Chem.* **1977**, *81*, 2288–2292.
[61] M. J. Frisch, G. W. Trucks, H. B. Schlegel, G. E. Scuseria, M. A. Robb, J. R. Cheeseman, G. Scalmani, V. Barone, B. Mennucci, G. A. Petersson, H. Nakatsuji, M. Caricato, X. Li, H. P. Hratchian, A. F. Izmaylov, J. Bloino, G. Zheng, J. L. Sonnenberg, M. Had, D. J. Fox, Gaussian Inc., Wallingford CT, **2013**.
[62] A. D. Becke, *J. Chem. Phys.* **1993**, *98*, 5648–5652.
[63] A. D. McLean, G. S. Chandler, *J. Chem. Phys.* **1980**, *72*, 5639–5648.
[64] V. Barone, M. Cossi, *J. Phys. Chem. A* **1998**, *102*, 1995–2001.
[65] L. Hermosilla, J. M. G. d. l. Vega, C. Sieiro, P. Calle, *J. Chem. Theory Comput.* **2011**, *7*, 169–179.
[66] R. Ditchfield, W. J. Hehre, J. A. Pople, *J. Chem. Phys.* **1971**, *54*, 724–728.
[67] M. S. Maier, K. Hüll, M. Reynders, B. S. Matsuura, P. Leippe, T. Ko, L. Schäffer, D. Trauner, *J. Am. Chem. Soc.* **2019**, *141*, 17295–17304.

Manuscript received: January 16, 2023
Accepted manuscript online: April 11, 2023
Version of record online: May 8, 2023

© 2023 The Authors. Chemistry - A European Journal published by Wiley-VCH GmbH

15213765, 2023, 35, Downloaded from https://chemistry-europe.onlinelibrary.wiley.com/doi/10.1002/chem.202300146 by CochraneAustria, Wiley Online Library on [22/08/2023]. See the Terms and Conditions (https://onlinelibrary.wiley.com/terms-and-conditions) on Wiley Online Library for rules of use; OA articles are governed by the applicable Creative Commons License